Invite Paper
Fall Technical Meeting
of the Eastern States Section of the Combustion Institute
Hosted by the University of Connecticut, Storrs, CT
Oct 9-12, 2011

Highly Turbulent Counterflow Flames: A Laboratory-Scale Benchmark for Turbulent Combustion Studies

Alessandro Gomez

Department of Mechanical Engineering and Materials Science
Yale Center for Combustion Studies
Yale University

This article discusses ongoing experimental research on turbulent nonpremixed and premixed flames in the counterflow configuration. Since the pioneering work of Weinberg's group at Imperial College in the '60s, the counterflow system has been the workhorse of laminar flame studies for decades. Recent developments have shown that it is also a promising benchmark for highly *turbulent* (Re_t ~1000) nonpremixed, partially premixed and premixed flames. Case studies will be discussed to demonstrate the compactness of the combustion region in nonpremixed flames and the versatility of the system in mimicking real flame effects in premixed flames, including heat loss and flame stratification. The system may offer significant advantages from a computational viewpoint, including: a) aerodynamic flame stabilization, near the interface between the two opposed jets, with ensuing simplifications in the prescription of boundary conditions; b) a fiftyfold reduction in the domain of interest as compared to conventional nonpremixed jet flames at the same Reynolds number; and c) on the order of one millisecond mean residence time, which is particularly useful for soot suppression in the combustion of fuels with modest-to-high soot propensity and for DNS/LES computational modeling.

1. Introduction

Concerns for climate change and pollution should lead in time to the development of robust and affordable renewable energy sources. Nevertheless, it is apparent that within a time frame of at least several decades there is no large-scale alternative the continued use of fossil fuels. Furthermore, the need for high energy density for transportation, especially in the case of aviation, suggests that it will be very difficult to replace liquid fuels in the long run. In a nutshell, at least within a time frame within which it is sensible to make predictions, combustion is here to stay.

In addition to oil and natural gas, alternative fuels are emerging to complement the fuel sources. Variations in fuel composition will pose new challenges to the clean and efficient implementation of combustion, which will necessitate studies in well-defined and well-controlled environments. Doing so in practical systems is very expensive experimentally and would provide modest feedback to optimize the system, in part because of limited diagnostic access. Computational Fluid Dynamics (CFD) is no panacea, although it is often mistakenly perceived as the magic bullet. Current engineering codes cannot predict *ab initio* emissions accurately, especially in the case of real fuels whose chemical kinetic characterization is not well developed.

These challenges suggest the need to study laboratory flames that are simpler than practical systems and yet able to cover operating regimes of practical relevance. This need is even more acute when dealing with real fuels with complex composition, which makes their complete kinetic characterization and modeling an impractical prospect. A natural candidate as a benchmark has been the jet flame on which the bulk of turbulent combustion research has been focusing for decades. In fact, even such a system has its shortcomings. To date, it has failed to bridge the two "camps" that have characterized virtually all modern combustion research: complex, and inevitably turbulent, fluid mechanics, but simple chemical kinetics (usually H_2 or CH_4 oxidation); or simple, and inevitably laminar, fluid mechanics, but complex kinetics, generally including mixtures of large hydrocarbons and aromatics. Tackling *complex fluid mechanics and complex chemical kinetics* has remained elusive experimentally because of complications associated with measurements, flame stabilization, and soot formation, among others, and computationally in part because of limited resources.

The focus of this contribution is on recent developments on a novel benchmark, a Counterflow Turbulent Flame (CTF) that can cover combustion regimes that are of relevance to practical combustors. The gains that this system may offer, as clarified in the subsequent sections, may enable significant advances through the integration of modern experimental methods and high performance simulation.

The counterflow system has been the workhorse of flame studies under laminar conditions for several decades, but it has received much less attention under *turbulent* conditions [1-17]. A drawback of the initial studies was that the turbulent Reynolds numbers were modest, at or below a typical value of 100, resulting in weak turbulence, which made these experiments of limited relevance to practical applications. By improving the design of the turbulence generation system [18] and selecting judiciously the feed stream composition, we increased the turbulent Reynolds numbers by one order of magnitude, with the system operating in a range of relevance to engines and gas turbines [19]. In the remainder of this article, I discuss innovative aspects of CTFs mostly qualitatively in an effort to reach a broad audience, that is not necessarily steeped in the turbulent combustion literature. A reprint of this work can be downloaded (No. 26) at http://www.eng.yale.edu/gomez-lab/pubs/index.html. Quantitative aspects of the work are detailed in the Refs. [20-25].

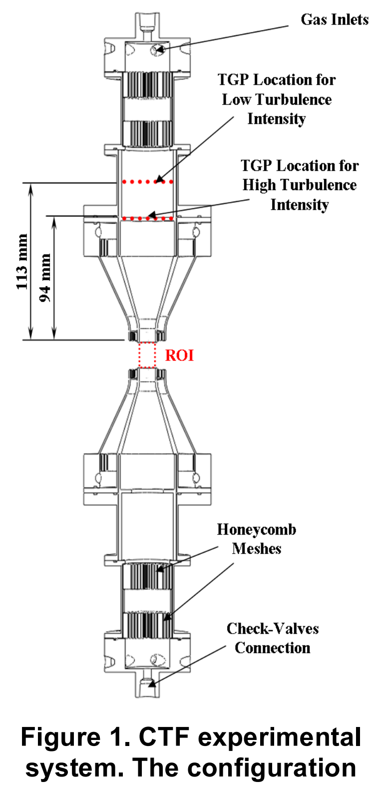

Figure 1. CTF experimental system. The configuration can be used either for nonpremixed combustion or for premixed (twin flames) conditions, with the region of interest (ROI) between the two nozzle outlets.

2. Experimental configuration and turbulence generation

The counterflow burner is realized by placing two exact copies of the same co-flowing jet nozzles approximately one inner nozzle diameter away from each other (Fig. 1). Each jet assembly consists of a 12.6 mm diameter inner nozzle and a 26.9 mm inner diameter outer nozzle. A special turbulence generation plate was found to be optimal in terms of flow uniformity at the exit section and turbulence intensity [18]. Different from [1-6, 10-12], the plate is positioned *upstream* of the contraction terminating with the burner outlet. An optional annular co-flow of nitrogen is used on both sides to quench partially the flame. The same burner can be used also under premixed and partially premixed conditions. In such a case two identical premixed streams are fed to top and bottom burner and turbulent twin premixed flames are established symmetrically, on average, with respect to the gas stagnation plane. Further details are in Ref. 19.

The achievement of large Reynolds numbers in this configuration is the result of two design improvements: the first is the introduction of a turbulence generation plate upstream of the burner contraction and the second is the operation with oxygen-rich streams to enhance flame stabilization even under conditions of very large strain rate. As a result both the mean velocity and the turbulence intensity were increased, which resulted in turbulent Reynolds number on the order of one thousand. The turbulence generation plate presented a convoluted central opening shaped as a 12-petal “daisy” (Fig. 2) with a 0.9 blockage. It was carefully designed with three goals: reaching high turbulent intensity in the stream of fresh reactants, avoiding the presence of anomalous frequencies in the turbulent power spectrum, and preserving the axisymmetric uniformity of the mean flow field [12]. Its selection was the result of extensive evaluations of several plate designs under cold conditions [18]. Typical turbulence intensities are on the order of 25% and can be varied by changing the distance between the plate and the nozzle outlet.

Figure 2. Turbulence generation plate

3. Nonpremixed and Partially Premixed Flames

Figure 3 shows nonpremixed flames under different conditions. Seeded olive oil droplets for PIV measurements disappear at 570K, leaving a dark region straddling the flame. With turbulence generators on both sides, intense flame wrinkling is shown with both turbulent fields interacting. Figure 3 (left) shows a case in which the two streams are separated by a hot reactive zone straddling the mixing layer, as typical of a robustly burning nonpremixed flames. By weakening the flame with increased inert dilution and higher strain rate, highly fluctuating strain rates induce local extinction in the flame, as indicated by the interruption in the droplet-free, dark area that is no longer simply connected (Fig. 3-right). These extinction events (highlighted circle in the picture) remain local and are symptomatic of conditions of partial premixing, since the unburned reactants have an opportunity to premix locally. When the extinction hole heals itself, conditions under which either turbulent edge flames are established or the mixture autoignites, as examined computationally in recent studies [26], can be studied systematically.

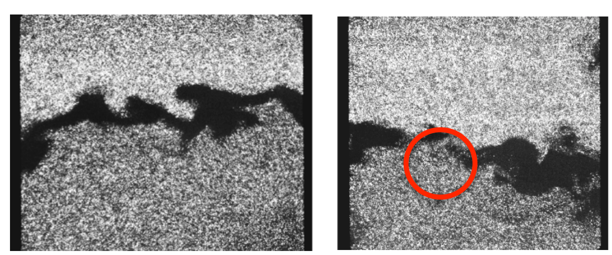

Figure 3. PIV raw images of seeded oil droplets showing robust burning (left) and evidence of local extinction/reignition (right).

The demonstrated turbulent Reynolds numbers range from a few hundreds to a few thousands. Under local extinction conditions, the Damköhler number based on the integral scale, $Da=(L/u')/(D/S_L^2)$, where u’ is a characteristic turbulent fluctuation velocity, L is the integral scale, and D/S_L^2 is a characteristic chemical time based on a mean diffusivity and the laminar flame speed, must be of unity order. For stable flames, this nondimensional number will be much larger. As a result, the experiment system covers the square domain highlighted in the Williams-Klimov diagram in Fig. 4. Importantly, it covers a subdomain of relevance to practical systems, such as Diesel engines and gas turbines (ovals in the same figure) [27], despite the fact that experiments are conducted in a bench-top burner.

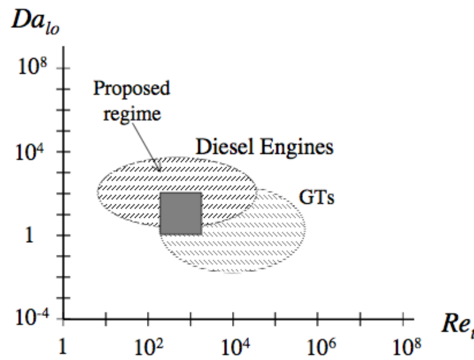

Figure 4. Nonpremixed combustion regimes

A distinct advantage of the counterflow configuration is the compactness of the domain in which combustion takes place. To prove this point, it is useful to compare it with that of the far more common jet flame that is abundantly documented in the literature. Figure 5 shows a comparison between long-exposure photographs of two C_2H_4 nonpremixed flame brushes, one in counterflow, the other as a piloted jet flame. Both flames operated at the same engineering Reynolds number (10,000) and turbulent Reynolds number (1000). Both pictures are reproduced in the same scale to evidence the dramatic difference, by a factor of roughly 50, in the cylindrical volume of the chemiluminescent regions in the two configurations. As mentioned earlier, the anticipated advantage is dramatic from a computational viewpoint. The volume reduction translates in potential computational cost savings of *two to three orders of magnitude*.

For a given computational cost (inclusive of time and memory requirements) the turbulent counterflow flame will permit the inclusion of increasingly more complex chemical kinetics. Larger molecular weight fuels have a high tendency to soot. Adding soot to turbulence would compound modeling challenges. In addition, laser diagnostics would be also adversely affected by the presence of soot and even of broadly fluorescent soot precursors, such as PAHs, that would complicate the implementation of laser induced fluorescence of commonly imaged combustion intermediates such as OH and CH. As a result, there is a dual experimental and computational need to keep soot formation at bay. In this context, there is one additional advantage that is intrinsic of the counterflow configuration: soot suppression. Healthy turbulence necessitates operating at strain rates on the order of 1000 s^{-1}, resulting in average residence times of one millisecond or less, which suppress the relatively slow soot chemistry.

The CTF advantage is also substantial in at least one other respect. The need for a piloted flame in the coflow configuration poses notorious problems computationally that are difficult to solve because one needs to pose realistic boundary conditions near the burner surface. The problem is completely circumvented in counterflow since the stabilization is aerodynamic, so long as adiabaticity is preserved. As the photograph in Fig. 5 shows, that is the case since the turbulent brush does not touch the boundaries and the preservation of adiabaticity is assured.

Figure 5. Same-scale long-exposure photographs of C_2H_4 nonpremixed flames at comparable cold Re_t ~ 10^3 in counterflow (left) and coflow (right)

For a more quantitative analysis, modeling is indispensible. In collaboration with the group of Professor Kempf (at the time, at Imperial College), we studied a turbulent non-premixed counterflow under both isothermal and reactive conditions, with turbulent Reynolds numbers reaching a value of 900 [23]. In this first study, the flame did not present evidence of local extinction, which is more challenging to model. Experimentally, Hot Wire Anemometry, twodimensional Particle Image Velocimetry (PIV) and OH Planar Laser Induced Fluorescence (PLIF) were applied. Computationally, Large-Eddy Simulations (LES) with a steady flamelet model were used to simulate both the flow inside the nozzles and in the opposed flow region, using three different grid resolutions (1.0-0.2mm, 0.5–70 million cells). Even though the prescription of detailed boundary conditions may necessitate the modeling of the flow within the nozzle, the cold flow in the nozzles can be decoupled from the reactive flow between them. Therefore, the anticipated computational advantages, as discussed in connection with Fig. 5 remain.

The extension of the computational domain to a region within the nozzles with no optical access revealed the mechanism by which the specially designed turbulence generating plate (TGP) and burner housing yield turbulence intensities well exceeding 20%, with the issuing of a turbulent jet from the plate buffeted by a recirculation region in the outer periphery.

The simulated and measured data were found to be in good agreement for first and second velocity moments, for the axial velocity autocorrelation function and for the normalized mean OH fluorescence, as shown in Fig. 6. The computed mixture fraction fluctuations look very similar to the negative spatial derivative (dotted line in Fig. 6e) of the mean mixture fraction, implying that the instantaneous mixing layer can be considered to be very thin compared to the amplitude of oscillation of the mixing layer in z-direction. With OH being a marker for the flame front, the mean OH concentrations along the centerline can also be interpreted as the distribution of the probability to find the flame at a position z. Figure 7 shows the mass fraction of OH between the nozzle exits at three instances from LES and PLIF images, demonstrating the range of flame morphologies that are typical of these flames with flat, thin, curved, and strongly

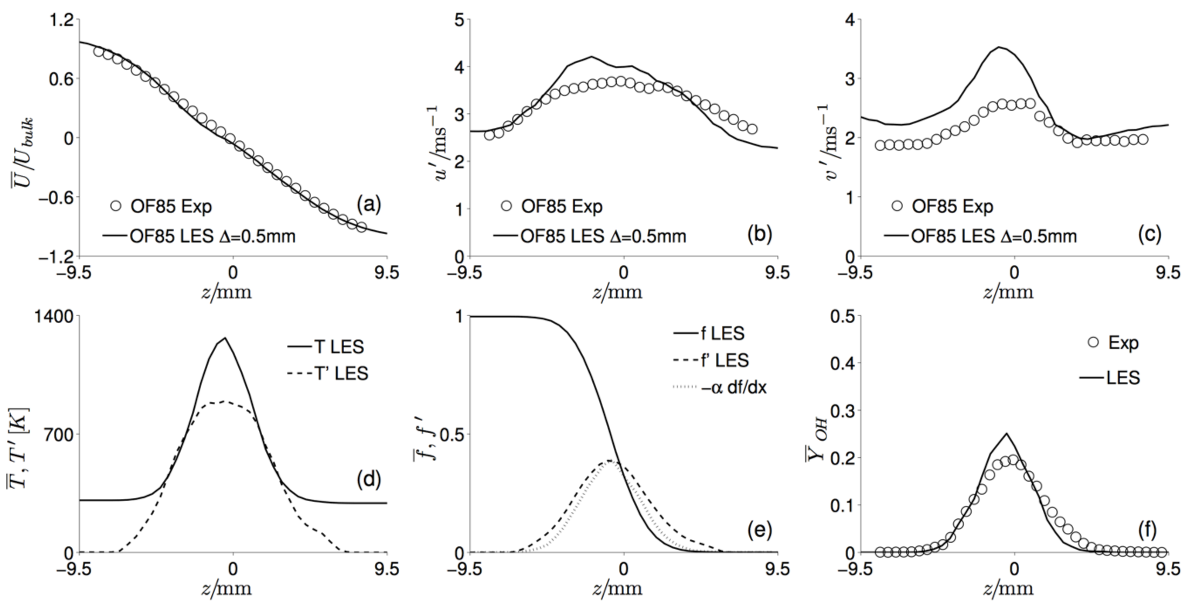

Figure 6. Comparison of experimental and computational data for a nonpremixed counterflow flame: (a) normalized mean axial velocity, (b) axial velocity fluctuation, (c) radial velocity fluctuation, (d) mean temperature and fluctuation, (e) mean mixture fraction, its first derivative scaled with α, and fluctuation, and (f) normalized OH concentration along the axis between the nozzle exits, relative to the stagnation plane at z=0.

corrugated flames, as well as flames that have locally thick regions. Both computational and experimental data show similar morphologies, which further contributes to the model validation.

These preliminary results are encouraging, but the comparison needs to be grounded on much more systematic work. This indeed is the goal of an on-going collaborative effort with the participation of Professor Stephen Pope (Cornell University) for the modeling component and of Dr. Jonathan Frank (Sandia National Laboratories) for advanced laser diagnostic applications.

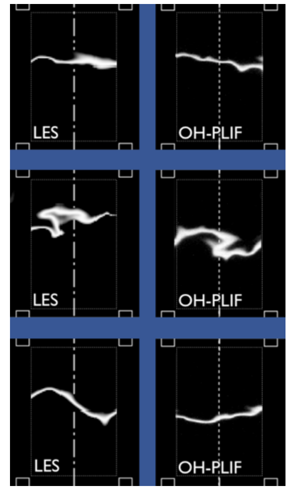

Figure 7. Instantaneous OH snapshots of the flame from LES and PLIF: white regions indicate higher concentrations of OH; dark regions indicate no presence of OH.

4. Premixed Flames

To orient the reader in the ensuing discussion, it is best to consider the premixed equivalent of Fig. 4, the so-called Borghi's diagram plotting the turbulent fluctuating velocity nondimensionalized with respect to a laminar flame speed versus the integral turbulent length scale nondimensionalized with respect to a laminar flame thickness. Different domains are highlighted in such a plot as shown in Fig. 8. One can distinguish the flamelet region in which the fundamental structure of a laminar flame is unperturbed by the turbulence that brings about a mere corrugation of such a structure. The non-flamelet regime, often called broken reaction zones regime or distributed reaction zones regime, covers the upper left section of the diagram. It corresponds to situations of distributed flame fronts or discontinuous flame sheets locally extinguished by turbulent eddies and is expected in very intense turbulence of relevance to practical applications. A turbulent Karlovitz number Ka_η, defined as the ratio of a relevant chemical timescale to the turnover time of the Kolmogorov microscale, is used to quantify the degree of turbulence/chemistry interaction and to define the boundary between regimes. Ka_η is expected to exceed a value of 100 in the non-flamelet regime, as marked by an oblique solid line at the boundary of the two domains [28]. Figure 8 shows also typical operating domains of gas turbines (orange oval) and IC engines (red oval). The green quadrilateral covers the range of conditions of CTF that can be stabilized in the premixed flame burners. Clearly, the CTF system manages to cover turbulent combustion regimes relevant to practical applications even under premixed conditions. Notice that conditions of strong turbulence and chemistry interaction in the non-flamelet regime are particularly challenging to reproduce in a laboratory scale burner and are rarely reported.

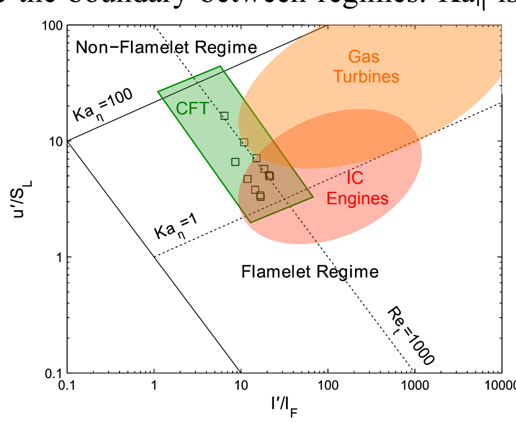

Figure 8. Borghi diagram of regimes of turbulent premixed combustion

As discussed earlier, when two counterflowing jets consist of identical premixed reactant mixtures are opposed to each other, two turbulent twin flames are stabilized on each side of the stagnation plane using the burner configuration in Fig. 1. However, the mutual influence of the two flames and their eventual merging at large strain rates is rather artificial and this twin flame configuration is ill suited to explore a wide range of Karlovitz numbers. For these reasons, we modified the burner and replaced the bottom half with a ceramic burner that passed the exhaust gases of a premixed flame stabilized in a preburner upstream, as in Fig. 9. In that way, a single turbulent counterflow flame could be systematically investigated in a configuration in which a fresh mixture was counterflown against combustion products. This configuration provides an opportunity to reach large Karlovitz numbers and has the additional advantage of mimicking other aspects of practical combustion, as explained below.

Shown in Fig. 8 are symbols of the experimental conditions investigated in the single premixed flame burner to date [22, 25, 29], with turbulent Reynolds number Re_t=O(1000) and turbulent Karlovitz number Ka_η ranging from unity to 400. Virtually all of the studied flames exhibited local extinction to various degrees. This phenomenon of torn flamelet is inherently associated with the non-flamelet regime. Clearly, the textbook value of Ka_η=100 grossly overestimates the size of the flamelet domain. This dramatic effect is the result of the introduction of real flame effects, namely, large strain rates, heat losses, that can be varied systematically in our burner by varying the temperature of the combustion products, and flame stratification effects that can be studied by varying the composition of the premixed flame in the preburner (Fig. 1) whose combustion products are counterflown to the fresh mixture. As a result, the equivalence ratio of the fresh, unburned mixture can differ from that of the flame in the preburner that affects the concentration of oxidizing species in the burnt products. The latter may affect local extinction, as highlighted in computational studies in laminar flames [21].

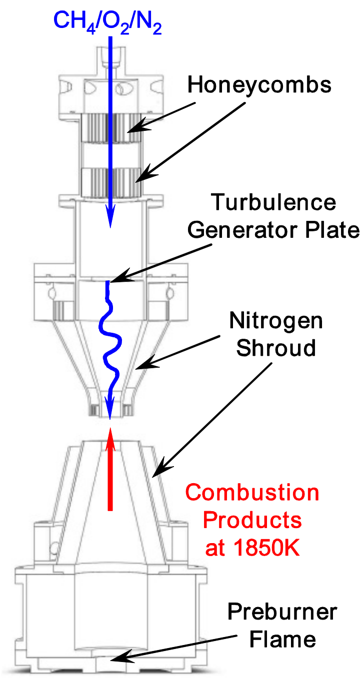

Figure 9. Configuration for single turbulent premixed flame. On the top, the burner is identical to that in Fig. 1. The bottom burner is made of ceramic cast and accommodates hot combustion products from a preburner.

A first consequence of these observations is apparent: the Borghi diagram that so far has provided a conceptual framework for the understanding of turbulent premixed flames will have to be redrawn in consideration of real flame effects that affect qualitatively the boundaries of the flamelet regime. Whether this can be done compactly in a similar two-dimensional diagram remains to be seen. Since the degrees of freedom to introduce real flame effects are numerous, either multidimensional plots or a preliminary theoretical scaling of these flames will be necessary.

As a quantitative case study of some of the paradoxes that we uncovered in the context of the Borghi's diagram, I show in Fig. 10 simultaneous imaging of two-photon CO-PLIF (first column), single-photon OH-PLIF (middle column) and their pixel-by-pixel product yielding a quantity proportional to the forward reaction rate (RR) of $CO + OH \rightarrow CO_2 + H$ reaction. These diagnostics were applied in the uniquely equipped laboratory of Dr. Frank at Sandia as part of an ongoing

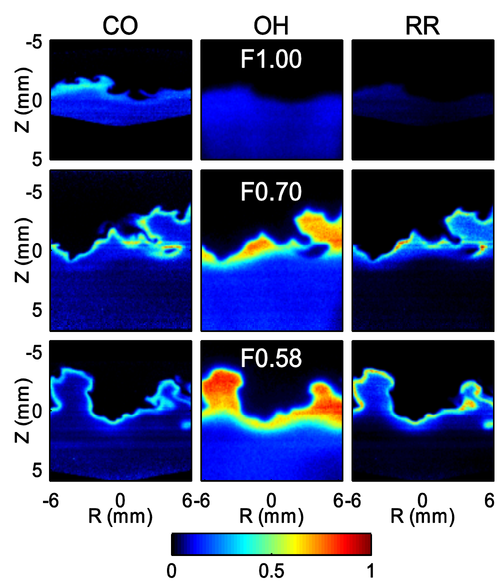

Figure 10. Simultaneous single-shot CO LIF, OH LIF, and CO+OH reaction rate images (left to right) for three flames, from stoichiometric to lean (top to bottom).

collaboration. The reaction rate imaging technique is described in detail elsewhere [30-31]. The top image row pertains to a stoichiometric flame (equivalence ration F=1.00) while the middle and bottom rows to two progressively leaner turbulent premixed flames. They were stabilized by counteflowing the fresh mixture to combustion products at 1800 K from a stoichiometric flame in the preburner. Despite the different stoichiometry all flames had the same unstrained laminar flame speed, at approximately 53 cm/s, through changes in inert concentration. Since the turbulence characteristics of the fresh mixture streams were identical for all flames, the turbulent burning regime was also the same, with a turbulent Reynolds number of 1050 and a Karlovitz number of approximately 5. The implication is that all flames occupy the same point in the Borghi's diagram in Fig. 8. Yet, the oxidation layer of the stoichiometric flame was extinguished, whereas the lean flames exhibited substantial evidence of CO conversion as indicated by the reaction rate images in the last column.

This anecdotal evidence is supported statistically by conditionally averaged profiles of the three variables imaged in Fig. 10 in all three flames. Figure 11 shows conditionally averaged flame-normal profiles that were calculated from 300 single shot measurements. The average CO LIF, OH LIF, and RR curves were normalized by their respective peak values for the leanest flame, F0.58. The averaged structures of flames F0.58 and F0.70 were similar to that of a laminar premixed flame. They are indicative of a flame propagating towards the stream of fresh reactants. The conditionally averaged OH LIF profile exhibits a steep gradient where the CO LIF profile reaches a maximum. As a result, the CO+OH reaction rate increases rapidly before decaying slowly downstream, which confirms the presence of oxidation layers in both F0.58 and F0.70. The conditionally averaged CO+OH reaction rate in F0.58 is larger than in F0.70, which implies that the chemically active oxidation layers of the latter are more frequently extinguished locally. Conversely, the oxidation layer is altogether absent in the conditionally averaged structure of flame F1.00. The smooth OH profile is the result of diffusion of the OH radical in the counterflowing products of combustion across the turbulent mixing layer. Therefore, the primary path of conversion of CO into CO_2 is virtually nonexistent in such a flame. In freely propagating flames, this lack of conversion would correspond to the loss of one third of the total heat release.

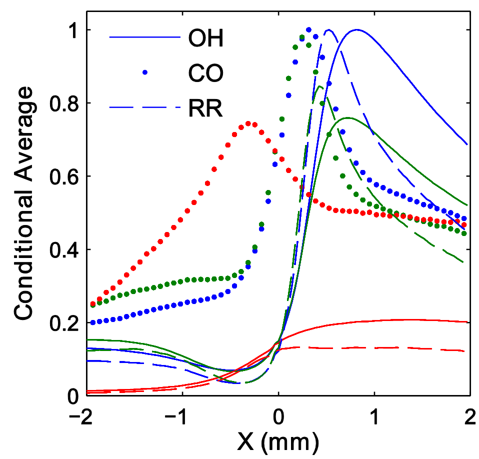

Figure 11. Conditionally averaged profiles of CO LIF (dotted), OH LIF(solid) and CO+OH reaction rate (dashed) as a function of the local normal to the flame front for three flames: F0.58 (blue), F0.70 (green) and F1.00 (red).

To aid the interpretation of the experiments, we numerically investigated the extinction of strained laminar premixed flames with compositions identical to those of the experiments [22]. The calculations corroborated the experimental results, indicating that the stoichiometric flame was the least robust and extinguished at the lowest strain rate [21]. Furthermore, extinction occurred when the flames were very close to the gas stagnation plane and the oxidation layer extended beyond it, towards the burnt product side. This case study exemplifies the remarkable insight that can be gained in the complexities of these flames even by *laminar* flame calculations that are routinely performed with commercial codes. They can help explaining the transition to the nonflamelet regime, in which the very structure of the flame is disrupted.

The quenching of the CO-to-CO_2 conversion observed in the stoichiometric case implies that in the absence of this conversion the entire flame is locally extinguished, as also confirmed by the laminar flame calculations and by more recent and yet unpublished measurements of heat release rate using the product of HCHO PLIF and OH PLIF images [29]. Remarkably, despite the modest value of the Karlovitz number, at approximately five, conditions pertaining to the non-flamelet regime are established, consistently with the stated need to redraw the boundary of this regime, as anticipated in the discussion of Fig. 8.

5. Coherent Structures and Instabilities

A potential problem associated with turbulent counterflow streams is the presence of large-scale instabilities that cause both up-and-down fluctuations as well as tilting of the mixing layer, and of the flame stabilized in its vicinity [20]. They can be easily seen even by naked eye or in high-speed movies of the flame chemiluminescence and in instantaneous snapshots of PLIF images. The origin of these instabilities is not well understood and is likely to be associated both with the turbulence generation mechanism, since they are generally not observed under laminar conditions, and with the counterflow configuration, since they are not found in the simple jet case. It is natural to wonder how they affect the turbulence. To shed light on this issue, the velocity field was measured by Particle Image Velocimetry (PIV) and analyzed using Proper Orthogonal Decomposition (POD), that is an effective mathematical tool for the detection of coherent structures in turbulence. POD performs a linear modal decomposition of the flow and is most efficient at capturing the modes with the largest kinetic energy on average [32].

An example of the type of data obtained by this analysis is presented in Fig. 12 showing the streamlines of the nine most energetic POD modes. Mode 0 corresponds to the mean flow, the sum of Mode 0 and Mode 1 yields the vertical displacement of the gas mixing layer, whereas the sum of Mode 0 and Mode 2 yields the tilting of the mixing layer. The coherent structures highlighted by the streamlines in the first nine modes are symmetric with respect to the centerline and the midplane between burners and, as such, are burner-specific. The first nine modes account for 92% of the total kinetic energy of the system. The vortical structures composing the higher POD modes are smaller, disorganized and distorted and constitute the incoherent turbulent background and the bulk of the vorticity RMS. Similar results were obtained under reacting conditions, in which case PIV/OH-

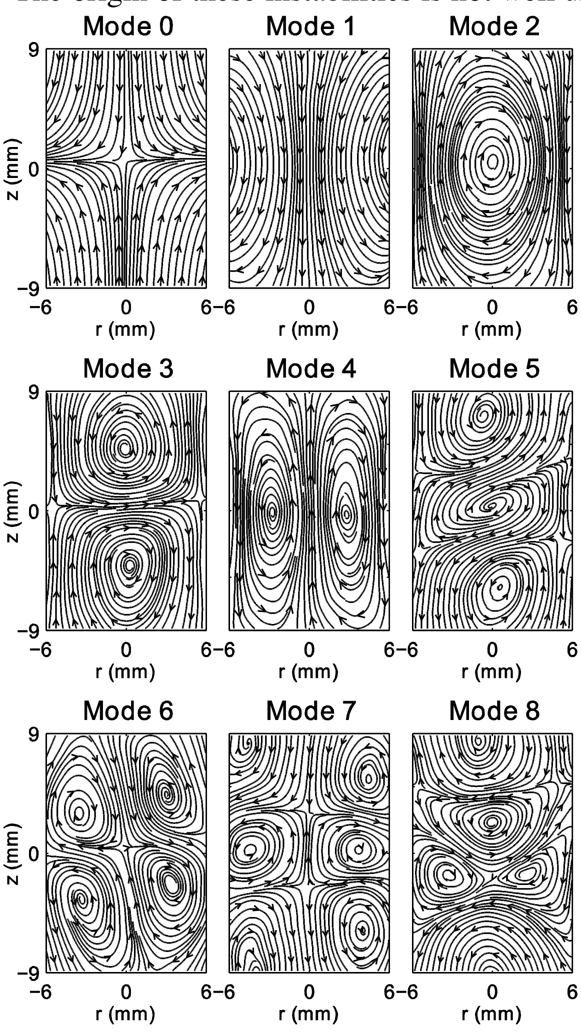

Figure 12. Streamlines of the nine most energetic POD modes under typical turbulent conditions

LIF measurements were synchronized and Extended POD (EPOD) of the OH-LIF images was used to complement the POD of the velocity measurements. In that way, we could study how the flame dynamics correlated with the turbulence coherent structures, similarly to Refs. [33]. This analysis confirmed that the large-scale displacements of the turbulent mixing layer induce similar simultaneous motions of the turbulent flames.

The fluctuations accompanying these large-scale motions of the gas mixing layer do affect the turbulence statistics. Figure 13 shows axial and radial components of the RMS velocity plotted in red and blue, respectively, along the burner centerline. RMS of the original velocity field (solid lines), the velocity fields from which the POD modes 1 and 2 were subtracted (dashed lines), and the incoherent flow field (dotted lines) are compared. The original flow field becomes significantly anisotropic near the plane of symmetry. The axial RMS velocity *v'* increases by 50% at the plane of symmetry whereas the radial component *u'* varies by less than 10% across the entire counterflow domain. At first, the unconditional RMS of *v'* could be interpreted as a gain of turbulent kinetic energy when turbulent eddies approach the turbulent mixing layer. However, when the velocity components of POD modes 1 and 2 are subtracted, *v'* becomes remarkably uniform along the burner centerline. *u'* is moderately affected by the subtraction. Therefore, the excess of turbulent fluctuations that is a recurrent source of discrepancy between experiments and models [34-36] largely results from the instability of the counterflow geometry rather than a mechanism of production of turbulent kinetic energy. Furthermore, the radial and axial velocity RMS of the incoherent flow field, also plotted in Fig. 5a, are found to be nearly identical to each other, suggesting that the incoherent flow field is much more isotropic, as compared to the original data. We conclude that the severe anisotropy of the original turbulent flow around the plane of symmetry is due to the presence of coherent structures and particularly to large-scale oscillations of the gas mixing layer. Although these coherent structures induce a significant amount of "apparent" turbulent fluctuations, they do not contribute to any loss/gain of turbulent vorticity.

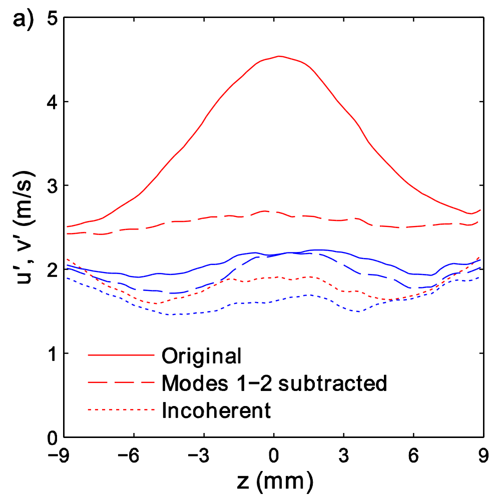

Figure 13. Radial (blue) and axial (red) velocity RMS, *u'* and *v'*, respectively. Solid lines: original velocity field; dashed lines: velocity field removed of POD modes 1 and 2; dotted lines: incoherent flow field.

A comparison of the power spectrum of hot wire measurements performed at the outlet of one of these nozzles reveals differences between the flow behavior as a simple jet and that when the jet is counterflown to an identical stream. The differences are present only at low frequencies, that is, below 300 Hz. In the first case, no oscillation or tilting of the jet is observable, which suggest that the difference in power spectra can be attributed to the presence of these coherent structures and instabilities. Analysis of high-speed movies of the turbulent counterflow system suggests that the instabilities prevail at frequencies on the order of 100 Hz or less. Since estimates of both the integral scale turnover time and the mean residence time suggest values significantly lower than the period associated with these frequencies, we conclude, then, that the instabilities are not part of the turbulence.

In the statistical analysis of the data, one can circumvent artifacts of the type discussed in connection with Fig. 13 by performing measurements conditional to the presence of the flame

[20, 22, 24, 25]. Nonetheless, it may be advantageous to suppress these instabilities altogether to lock the flame in place and observe aspects of flame/turbulence interaction with higher spatial resolution. In view of the slow frequencies involved, it should be feasible to implement a sufficiently fast active-control strategy, but the broadband nature of the instability makes the task challenging. Experiments are under way to explore this active control option.

Concluding Remarks

In summary, we reviewed key aspect of highly turbulent counteflow flames providing a convenient system for the study of phenomena relevant to practical combustion systems. Principle advantages that should make it an ideal benchmark for joint experimental and computational studies include:

1. Simplicity and versatility of the experimental set-up, allowing for the exploration of a range of stoichiometries (from non-premixed to premixed) and accessing a broad range of conditions (in terms of Re, Da and Ka), including non-flamelet regimes, at turbulent Reynolds numbers of practical relevance;
2. Flame compactness and short residence times, allowing for highly resolved simulations in a relatively small computational domain;
3. Elimination of the influence of nearby surfaces and/or pilot flames to anchor the flame, which removes a significant source of modeling uncertainty; and
4. Soot suppression.

Acknowledgments

I am indebted first and foremost to the two graduate students who did most of the work as part of their doctoral theses: Drs. Gianfilippo Coppola and Bruno Coriton. I am also grateful to Dr. Jonathan H. Frank (Sandia National Laboratories, CRF), who collaborated by applying advanced laser diagnostics that otherwise would have been out of our reach, and to Professor Amable Liñán (Politecnico of Madrid), who, through countless conversations in his periodic visits at Yale, has been sharpening my understanding of flames and that of my students. The support of the American Chemical Society (ACS) through Grant PRF#46991-AC9, of NSF (Grant #1060762.1.D1692.652001, Dr. Arvind Atreya, Program Director), and of the U.S. Department of Energy to Dr. Frank is gratefully acknowledged.

References

[1] Mastorakos, E., Taylor, A.M.K.P., and Whitelaw, J.H., 1992, "Comb. Flame, Vol. 91, pp. 40-52.
[2] Mastorakos, E., Taylor, A.M.K.P., and Whitelaw, J.H., 1992, *Comb. Flame*, Vol 91, pp.55-64.
[3] Mastorakos, E., Taylor, A.M.K.P., and Whitelaw, J.H., 1995, Comb. Flame, Vol. 102, pp. 101-114.
[4] Kostiuk, L.W., Bray, K.N.C., and Chew, T.C., 1989, Comb. Sci. and Technol., 64, pp. 233-241.
[5] Kostiuk, L.W., Bray, K.N.C., and Cheng, R.K., 1993, The Combustion Institute, pp. 377-395.
[6] Kostiuk, L.W., Bray, K.N.C., and Cheng, R.K., 1993, *Comb. Flame,* Vol. 91, pp. 396-409.
[7] Erkstein, J., Chen, J.Y., Chou, C.P., and Janicka, J., 2000, *Proceedings of the Combustion Institute,* Vol. 28, pp. 141-148.
[8] Maury, Frederic A., and Libby, Paul A., 1995, *Comb. Flame*, Vol. 102, pp. 341-345.
[9] Kempf, A., Forkel, H., Chen, J.Y., Sadik, A., and Janicka, J., 2000, *Proceedings of the Combustion Institute,* Vol. 28, pp. 35-40.
[10] D. Geyer, A. Dreizler, J. Janicka, A.D. Permana and J.Y. Chen, 2005, *Proceedings of the Combustion Institute,* Vol. 30, pp. 711-718.

[11] D. Geyer, A. Kempf, A. Dreizler, J. Janicka, 2005, *Proceedings of the Combustion Institute,* Vol. 30, pp. 681-689
[12] Geyer, D, Kempf, A, Dreizler, A, et al , *Comb. Flame,*" Vol. 143, pg. 524 – 548.
[13] Bray, K.N.C., Champion, Michel, Libby, Paul A., 1994, "Flames in Stagnating Turbulence", in Turbulent Reacting Flows, (Libby, P. and Williams, Forman A., Eds.), Academic Press.
[14] Bray, K.N.C., Champion, Michel, Libby, Paul A., 1998, *Comb. Flame,* Vol. 112*,* pg. 635-654.
[15] Bray, K.N.C., Champion, Michel, and Libby, Paul A., 2000, *Comb. Flame*, Vol. 120, pp. 1-18.
[16] Sardi, K., Taylor, A.M.K.P., and Whitelaw., J.H., 1998, J. Fluid Mech., Vol. 361, pp. 1-24
[17] Lipatnikov, A.N. and Chomiak, J., 2002, Combust. Sci and Tech, Vol 174, pp. 3-26.
[18] G.F. Coppola, B. Coriton, B., A. Gomez, *Experimental Thermal and Fluid Science* 33 (2009) 1037-1048 (2009)
[19] G.F. Coppola, B. Coriton, B., A. Gomez, *Combust. Flame* 157 (2009) 1834-1843.
[20] G. Coppola, G., A. Gomez, *Physics of Fluids*, 22 (2010) 105101.
[21] B. Coriton, M.D. Smooke, M.D., A. Gomez, *Combust. Flame,* 157 (2010) 2155-2164.
[22] B. Coriton, B., J.H. Frank, A.G. Hsu, M.D. Smooke, A. Gomez, *Proceedings of the Combustion Institute*, 33 (2011) 1647-1654.
[23] M.W.A. Pettit, B. Coriton, B., A. Gomez, A.M. Kempf, *Proceedings of the Combustion Institute*, 33 (2011) 1391-1399.
[24] B. Coriton, A. Gomez, "POD Analysis of Coherent Structures in Non-reactive and Reacive Turbulent Opposed Jets," in preparation (2012).
[25] B. Coriton, B., J.H. Frank, A. Gomez, Presented at the 7th US National Combustion Meeting, Atlanta, GA, 2011
[26] J.H. Chen, E.R. Hawkes, R. Sankaran, S.D. Mason, H.G. Im, *Combust. Flame,* 145 (2006) 128-144.
[27] Williams, F.A., 2000, "Some Recent Studies in Turbulent Combustion," in Smart Control of Turbulent Combustion, (Yoshida, A., Ed.) *Springer-Verlag Tokyo*, pp. 1-12.
[28] N. Peters, *Turbulent Combustion*, Cambridge University Press, Cambridge, England, 2000.
[29] B. Coriton, J.H. Frank, A. Gomez, unpublished data
[30] Frank, J.H., Kaiser, S.A., Long, M.B., Proc. Combust. Inst. 29, (2002) 2687-2694.
[31] Rehm, J.E., Paul, P.H., Proc. Combust. Inst. 28, (2000) 1775-1782.
[32] L. Sirovich, Quart. J. Appl. Math. 45, 519 (1987).
[33] J. Borée, Exp. Fluids 35, 188 (2003).
[34] Y.H. Im, K.Y. Huh and K.Y. Kim, J. Fluids Eng. 124, 706 (2002).
[35] E. Korusoy and J.H. Whitelaw, Int. J. Numer. Methods Fluids 46, 1069 (2004).
[36] R.P. Lindstedt, D.S. Luff and J.H. Whitelaw, Proc. Combust. Inst. 31, 1459 (2007).